FIG. 1 (color online).   (a) plots the contact function Eq. (3.4) for two pairs of three-dimensional ellipsoids taken from a search for binaries consisting of nonspinning compact objects characterized by parameters (t_c, τ_0, τ_3) [see Sec. V, in particular, Eq. (5.4)]. (b)–(d) are the projections of the ellipsoids in (t_c, τ_0), (t_c, τ_3), and (τ_0, τ_3) orthogonal planes, respectively. Solid lines refer to the case of nonoverlapping ellipsoids and dashed lines are for overlapping (i.e., coincident) triggers. Note that in the latter case the maximum of the contact function is ≤ 1, which is the test that is carried out to determine if a pair of triggers are in coincidence.

ternally. Figure 1 shows the contact function in the case of overlapping and nonoverlapping ellipsoids.

In the "coincidence" data-analysis paradigm, given triggers from N detectors ($N \geq 2$), one draws up a list of "coincident triggers" for further analysis to test their significance. The simplest coincident triggers consist of those which have "consistent" parameters in two detectors (two-way coincidence). Testing for two-way coincidences for triggers from colocated detectors (e.g., the two LIGO detectors at Hanford) can be accomplished by a single test of Eq. (3.5) on a pair of triggers.

When the detectors are noncolocated, one needs to allow for a nonzero "time-of-flight" delay between the trigger arrival times. One assumes that the GW signals travel at the speed of electromagnetic radiation in vacuum c and the maximum allowed time delay is then set to $\pm \Delta / c$, where Δ is the distance between the two detectors. As far as the geometrical picture of the coincidence test is concerned, for the noncolocated case one needs to test for the overlap

of a "cylindrical" volume (of length $2\Delta/c$ along the time dimension) and an ellipsoid.[7] In practice, however, the test can be carried out iteratively by adding discrete time delays to the trigger (spanning the allowed time delay) from one detector and testing for the overlap condition against the trigger from the other detector, keeping the latter fixed in time. The discrete time step can be set to the inverse of the sampling frequency of the time series. The fact that the overlap test is computationally cheap allows for such a brute-force implementation strategy to be viable.

These 2-way coincident triggers can now be used as building blocks to construct more complex coincidence triggers that have consistent parameters over three or more interferometers (3-way, ..., n-way coincidence triggers). For example, the set of triggers (T_A, T_B, T_C) can be

---

[7] Note that, in the case of an externally triggered search, where the position of the source is known, we can use a fixed time delay for noncolocated detectors.

classified as 3-way coincident if (T_A, T_B), (T_B, T_C), and (T_A, T_C) 2-way coincident pairs exist. Here again, the subscripts $A \neq B \neq C$ are labels on interferometers. This idea can be generalized to determine the list of n-way coincident triggers given the list of $(n - 1)$-way coincidences. It is useful to note that Eq. (3.5) is the only test we need in order to build the entire hierarchy of coincidence triggers.

We conclude this section by drawing attention to two practical issues in implementing this geometrical coincidence test. The first has to do with the algorithm one uses to draw up two-way coincidences. Given the set of triggers from two detectors, one can (a) work with time-ordered triggers and (b) find the maximum length of the bounding box of the ellipsoid along the time dimension over all the triggers such that for any trigger from one detector, the test for overlap is carried out only if a trigger from the other detector occurs at a time that is within twice this interval. This approach greatly reduces the overall number of overlap tests required to find two-way coincidences. The expression for the length of the sides of the bounding box can be algebraically determined given the shape matrix of the triggers and is explicitly given for 2 and 3 dimensions in the next section.

The second point is about the numerical implementation of the test of the overlap of ellipsoids where we maximize the contact function over a single parameter λ. Evaluation of the contact function involves matrix inversion which can be computationally quite expensive. Under these circumstances, prior knowledge of the inverse of trigger shape matrices can prove to be more efficient than on-the-fly computation. Brent's minimization method [43,44] is particularly suitable for fast convergence to the maxima given the well-behaved nature of the contact function and is available as part of the GNU Scientific Library [45].

IV. EXPECTED REDUCTION IN FALSE ALARM RATE

Next, let us consider the reduction in the false alarm rate as a result of using ellipsoidal windows as opposed to rectangular windows.[8] In order to achieve false dismissal probability less than or equal to $1 - P$, a rectangular window has to be at least as large as the box that encloses the ellipsoid. Now the volume of an n-dimensional ellipsoid ($n \geq 2$) whose semiaxes are a_k, $k = 1, \ldots, n$, is given by a recursive formula:

$$V_n = \frac{2\pi V_{n-2}}{n} \prod_{k=1}^{n} a_k, \quad \text{where } V_0 = 1, \quad V_1 = 2.$$

(4.1)

On the other hand, the smallest volume an n-dimensional

---

[8]This discussion again assumes that false alarms are due to accidental coincidences between otherwise uncorrelated triggers.

box that encloses the ellipsoid would be

$$U_n = \prod_{k=1}^{n} (2a_k) = 2^n \prod_{k=1}^{n} a_k,$$

(4.2)

where a factor of 2 arises since a_k are semimajor axes and the side lengths of the enclosing box will be twice that value. Thus, the rectangular box's volume is larger than that of the ellipsoid by the factor

$$r \equiv \frac{U_n}{V_n} = \frac{n 2^{n-1}}{\pi V_{n-2}}.$$

(4.3)

Thus, in 2, 3, and 4 dimensions the savings are $4/\pi$, $6/\pi$, and $32/\pi^2$, respectively. However, the real factor could be far greater as the error ellipsoids are generally not oriented along the coordinate axes.

When the ellipsoid is not aligned with the coordinate axes, which will be the case when there are correlations between the different parameters, the side lengths of the bounding box are given by maximizing each coordinate axis over the entire ellipsoidal surface as follows. Starting from Eq. (2.17) one can express the first of the coordinates $p \equiv p^1$ in terms of the other coordinates:

$$g_{11}p^2 + 2g_{1i}pp^i + g_{ij}p^ip^j - \left(\frac{r}{\rho}\right)^2 = 0,$$

$$i, j = 2, \ldots, n,$$

(4.4)

which can be solved to obtain

$$p_\pm = \frac{1}{g_{11}}[-g_{1i}p^i \pm \sqrt{(g_{1i}g_{1j} - g_{11}g_{ij})p^ip^j + (g_{11}r^2/\rho^2)}].$$

(4.5)

For our purposes we only need the "plus" solution. One can then set up $n - 1$ equations in as many variables by demanding that $\partial p_+/\partial p^k = 0$, which gives

$$\left[\frac{(g_{1i}g_{1k} - g_{11}g_{ik})(g_{1j}g_{1k} - g_{11}g_{jk})}{g_{1k}^2} - (g_{1i}g_{1j} - g_{11}g_{ij})\right]$$

$$\times p^ip^j = g_{11}\frac{r^2}{\rho^2}.$$

(4.6)

These are again quadratic equations that must be solved (simultaneously) for the coordinates p^j, $j = 2, \ldots, n$. The resulting (positive) roots, denoted p_1^j can be substituted in Eq. (4.4) to obtain the half side length of the ellipse. We shall next give explicit expressions for the side lengths of the enclosing box in two and three dimensions. In higher dimensions the expressions are rather cumbersome but the general procedure outlined above can be used to compute the volume of the bounding box in all cases.

The side lengths of the bounding box are given in two dimensions by

$$x = 2\sqrt{\frac{\bar{g}_{22}}{|\bar{g}|}}, \qquad y = 2\sqrt{\frac{\bar{g}_{11}}{|\bar{g}|}}, \qquad (4.7)$$

and in three dimensions by

$$x = 2\sqrt{\frac{(\bar{g}_{23}^2 - \bar{g}_{22}\bar{g}_{33})\bar{g}_{22}}{(\bar{g}_{12}\bar{g}_{23} - \bar{g}_{22}\bar{g}_{13})^2 - (\bar{g}_{23}^2 - \bar{g}_{22}\bar{g}_{33})(\bar{g}_{12}^2 - \bar{g}_{11}\bar{g}_{22})}},$$

$$y = 2\sqrt{\frac{(\bar{g}_{13}^2 - \bar{g}_{11}\bar{g}_{33})\bar{g}_{11}}{(\bar{g}_{12}\bar{g}_{13} - \bar{g}_{11}\bar{g}_{23})^2 - (\bar{g}_{13}^2 - \bar{g}_{11}\bar{g}_{33})(\bar{g}_{12}^2 - \bar{g}_{11}\bar{g}_{22})}},$$

$$z = 2\sqrt{\frac{(\bar{g}_{12}^2 - \bar{g}_{11}\bar{g}_{22})\bar{g}_{11}}{(\bar{g}_{12}\bar{g}_{13} - \bar{g}_{11}\bar{g}_{23})^2 - (\bar{g}_{12}^2 - \bar{g}_{11}\bar{g}_{22})(\bar{g}_{13}^2 - \bar{g}_{11}\bar{g}_{33})}}.$$
$$(4.8)$$

V. APPLICATION TO COALESCING BINARIES

Inspiralling compact binaries are one of the most promising candidates for detection by the laser interferometric detectors. It will, therefore, be interesting to investigate the gains of using the new coincidence method in such searches. For the purpose of our discussion, it will suffice to use a simple model of the signal. We shall use the Fourier representation of the waveform from a binary consisting of nonspinning compact objects on a quasicircular orbit in which post-Newtonian corrections to the amplitude are neglected, but corrections to the phase are included to the desired order. This waveform is calculated using the stationary phase approximation, and is of the form:

$$\tilde{h}(f) = \frac{AM^{5/6}}{D\pi^{2/3}}\sqrt{\frac{5\eta}{24}}f^{-7/6}\exp\left[i\Psi(f; t_C, \phi_C, k) + i\frac{\pi}{4}\right],$$
$$(5.1)$$

$$\Psi(f) = 2\pi f t_C + \phi_C + \sum_k \lambda_k f^{(k-5)/3}, \qquad (5.2)$$

where M is the total mass of the system, and η is the symmetric mass ratio, which is defined as $\eta \equiv m_1 m_2 / M^2$. D is the distance to the source, and A is a constant which depends on the relative orientations of the detector and the binary orbit, and t_C and ϕ_C are as defined in Sec. II A. Waveforms of this type at second post-Newtonian order [46,47] have been used in previous searches for binary neutron star inspirals [12], and are currently being used in searches for compact binary inspirals with a total mass of $<35M_\odot$ [41]. Moreover, the metric computed for such a waveform has been shown to be approximately valid for a range of physical approximants [48,49]. At the 2PN order, the coefficients λ_k are given by the following expressions:

$$\lambda_0 = \frac{3}{128\eta(\pi M)^{5/3}}, \qquad \lambda_1 = 0,$$

$$\lambda_2 = \frac{5}{96\pi\eta M}\left(\frac{743}{336} + \frac{11}{4}\eta\right), \qquad \lambda_3 = \frac{-3\pi^{1/3}}{8\eta M^{2/3}}, \quad (5.3)$$

$$\lambda_4 = \frac{15}{64\eta(\pi M^{1/3}}\left(\frac{3058673}{1016064} + \frac{5429}{1008}\eta + \frac{617}{144}\eta^2\right).$$

The metric required for determining coincidence in the case of nonspinning binaries is that in the three-dimensional space of (t_C, τ_0, τ_3), where τ_0 and τ_3 are the chirp times, which are a convenient way of parametrizing the masses of the binary system. They are given by

$$\tau_0 = \frac{5}{256\pi f_L\eta}(\pi M f_L)^{-5/3},$$
$$\tau_3 = \frac{1}{8f_L\eta}(\pi M f_L)^{-2/3}, \qquad (5.4)$$

where f_L is the frequency below which no appreciable signal can be detected due to rising detector noise at low frequencies.

In obtaining the metric, it proves to be more convenient to use parameters $(t_C, \theta_1, \theta_2)$, where $\theta_1 \equiv 2\pi f_L\tau_0$, and $\theta_2 \equiv 2\pi f_L\tau_3$. This metric was obtained by Owen in [35]. Here, Eq. (2.6) was used, and the phase ϕ_C maximized over to give the expression for the metric:

$$g_{\alpha\beta} = \frac{1}{2}(\mathcal{J}[\psi_\alpha\psi_\beta] - \mathcal{J}[\psi_\alpha]\mathcal{J}[\psi_\beta]), \qquad (5.5)$$

where ψ_α is the derivative of the Fourier phase of the inspiral waveform with respect to parameter θ_α. $\mathcal{J}$ is the moment functional of the noise power spectral density (PSD), which is defined for any function $a(x)$ as

$$\mathcal{J}(a) \equiv \frac{1}{I(7)}\int_{x_L}^{x_U}\frac{a(x)x^{-7/3}}{S_h(x)}dx. \qquad (5.6)$$

$I(q)$ is the qth moment of the noise PSD, which is defined by

$$I(q) \equiv S_h(f_0)\int_{x_L}^{x_U}\frac{x^{-q/3}}{S_h(x)}dx, \qquad (5.7)$$

where $x \equiv f/f_0$, with f_0 being a fiducial frequency used to set the range of the numerical values of the functions contained in the integrals. The value of x_L is chosen so that the contribution to the integral for values below x_L would be negligible. $x_U \equiv f_U/f_0$, where f_U is the ending frequency of the inspiral waveform in question. In deriving the explicit expression for the metric, the starting point is the Fourier phase of the waveform in the form [48]:

$$\begin{aligned}\Psi(f; t_C, \theta_1, \theta_2) = {}& 2\pi f t_C + a_{01}\theta_1 x^{-5/3} + [a_{21}(\theta_1/\theta_2) \\ & + a_{22}(\theta_1\theta_2^2)^{1/3}]x^{-1} + a_{31}\theta_2 x^{-2/3} \\ & + [a_{41}(\theta_1/\theta_2^2) + a_{42}(\theta_1/\theta_2)^{1/3} \\ & + a_{43}(\theta_2^4/\theta_1)^{1/3}]x^{-1/3}, \qquad (5.8)\end{aligned}$$

where the coefficients a_{km} are given by

$$a_{01} = \frac{3}{5}, \qquad a_{21} = \frac{11\pi}{12}, \qquad a_{22} = \frac{743}{2016}\left(\frac{25}{2\pi^2}\right)^{1/3},$$

$$a_{31} = \frac{-3}{2}, \qquad a_{41} = \frac{617}{384}\pi^2, \qquad a_{42} = \frac{5429}{5376}\left(\frac{25\pi}{2}\right)^{1/3},$$

$$a_{43} = \frac{15\,293\,365}{10\,838\,016}\left(\frac{5}{4\pi^4}\right)^{1/3}. \qquad (5.9)$$

Using the above in Eq. (5.5), one can find an explicit expression for the metric. The expression can be obtained [48] by utilizing the fact that, since the Fourier phase is a polynomial function, $\mathcal{J}$ can be expanded in terms of normalized moments J, where

$$J(p) \equiv \frac{I(p)}{I(7)}. \qquad (5.10)$$

To assess the potential gains of using this coincidence method for inspiral analysis, it is useful to consider the

difference in volume between the ellipsoidal region defined by $\bar{g}$, and its bounding box aligned with the coordinate axes (t_C, τ_0, τ_3). This ratio can be calculated with the help of Eqs. (4.8). Figure 2 shows how this ratio varies across the (τ_0, τ_3) space in the case of Initial and Advanced LIGO, Virgo and Einstein Telescope (a third generation European detector that is currently being designed). It can be seen that for most of the parameter space, the volume of the bounding box is an order of magnitude larger than the volume of the ellipsoid; however, in certain regions, corresponding to high masses, this ratio can be as large as 2 orders of magnitude. This suggests that significant reductions of the background can be achieved by using ellipsoidal windows. Runs on example data sets suggest that in practice, the reduction in background coincident triggers due to using such a coincidence method will be a factor of ~ 10.

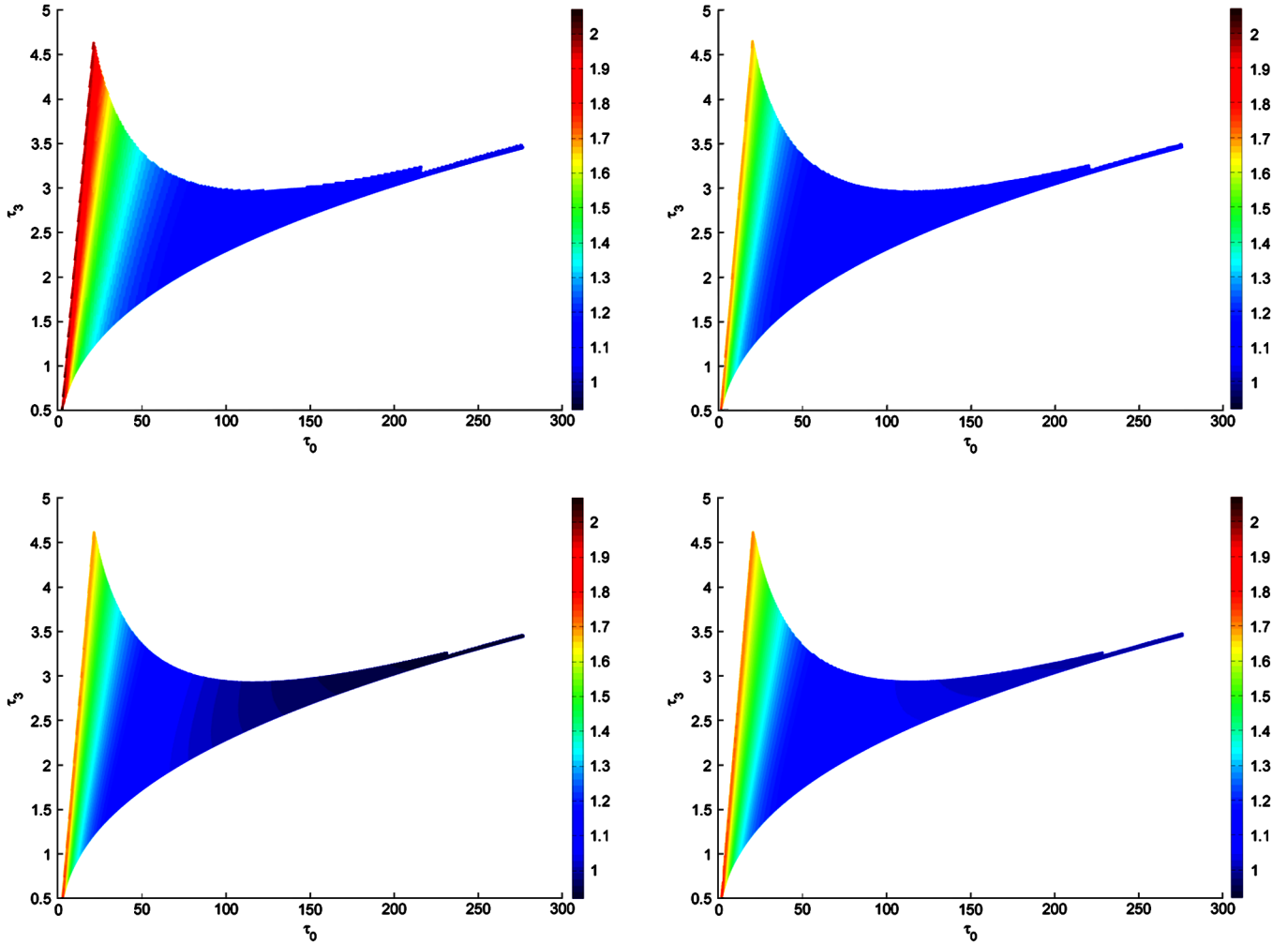To assess the improvement in the confidence in any candidate detection, it is helpful to look at how reducing

FIG. 2 (color online). The $\log_{10}$ of the ratio of the volume of the bounding box to the volume of the ellipsoid as a function of location in (τ_0, τ_3) space. The plots shown are (clockwise from top right) for the initial LIGO, advanced LIGO, Virgo, and Einstein Telescope. The low frequency cutoff is chosen to be 20 Hz.

the background rate by a factor of k will improve the odds O of a detection

$$O(h \mid D) = \frac{P(h \mid D)}{P(0 \mid D)}, \qquad (5.11)$$

where $P(h \mid D)$ is the posterior probability of a signal h being present if the set of triggers D has been obtained, and $P(0 \mid D)$ is the probability of there being no signal given D. We take the accidental trigger rate to be a Poisson process, with a trigger rate prior to reduction λ. Assuming that the detection efficiency is not affected by the reduction in the trigger rate, we see that the odds improve by the following factor:

$$\frac{O(h \mid D)_{\lambda/k}}{O(h \mid D)_\lambda} = \frac{1 - e^{-\lambda T}}{1 - e^{-\lambda T/k}}, \qquad (5.12)$$

where T is the duration of the run.

After reducing the false alarm rate by a factor k, the odds of a signal being present improve by a factor which depends on how high the false alarm rate was to start with. If the initial false alarm rate is low ($\lambda T \ll 1$), the improvement in the odds approaches the factor k. However, for high false alarm rates, the improvement becomes less marked, tending to a factor of 1 as $\lambda T \to \infty$.

VI. SUMMARY AND CONCLUSIONS

A new method of coincidence analysis is proposed in which, instead of the rectangular windows on parameters conventionally used, ellipsoidal windows are employed based on the metric defined on the signal manifold. This allows us to use windows of appropriate size depending on the location in the parameter space, instead of using a phenomenological ''best fit'' choice of windows across the entire space. The algorithm has a massive practical advantage in that it requires the tuning of only one parameter irrespective of the number of dimensions of the parameters. This contrasts with the conventional method that required us to tune nearly as many parameters as the dimension of the parameter space. In addition, the method allows us to take into account covariances between parameters, thus significantly reducing the volume enclosed within the windows. In particular, for the case of nonspinning compact binary coalescence in Initial LIGO, it is expected that the use of such a method will reduce the background rate of coincident triggers by roughly an order of magnitude. By also incorporating SNR dependence into the size of the windows, the background of high-SNR events can be reduced even further.

The algorithm has been implemented in C code in the LSC Algorithm Library (LAL) [50]. An implementation in (t_C, τ_0, τ_3) space, as in Sec. V, using SNR-independent windows, is being employed in the search for compact binary coalescence in S5 data. This implementation is referred to as *e-thinca* [41].

[1] B. Abbott *et al.* (LIGO Scientific Collaboration), Nucl. Instrum. Methods Phys. Res., Sect. A **517**, 154 (2004).

[2] F. Acernese *et al.*, Classical Quantum Gravity **23**, S635 (2006).

[3] H. Luck *et al.*, Classical Quantum Gravity **23**, S71 (2006).

[4] A. Pai, S. Dhurandhar, and S. Bose, Phys. Rev. D **64**, 042004 (2001).

[5] S. Bose, S. V. Dhurandhar, and A. Pai, Pramana **53**, 1125 (1999).

[6] L. S. Finn, Phys. Rev. D **63**, 102001 (2001).

[7] N. Arnaud *et al.*, Phys. Rev. D **68**, 102001 (2003).

[8] P. Jaranowski and A. Krolak, Phys. Rev. D **49**, 1723 (1994).

[9] P. Jaranowski and A. Krolak, Classical Quantum Gravity **13**, 1279 (1996).

[10] H. Tagoshi *et al.*, Phys. Rev. D **75**, 087306 (2007).

[11] B. Abbott *et al.* (LIGO Scientific Collaboration), Phys. Rev. D **69**, 122001 (2004).

[12] B. Abbott *et al.* (LIGO Scientific Collaboration), Phys. Rev. D **72**, 082001 (2005).

[13] B. Abbott *et al.* (LIGO Scientific Collaboration), Phys. Rev. D **72**, 082002 (2005).

[14] B. Abbott *et al.* (LIGO Scientific Collaboration), Phys. Rev. D **73**, 062001 (2006).

[15] N. Arnaud *et al.*, Phys. Rev. D **65**, 042004 (2002).

[16] H. Mukhopadhyay, N. Sago, H. Tagoshi, S. Dhurandhar, H. Takahashi, and N. Kanda, Phys. Rev. D **74**, 083005 (2006).

[17] B. Abbott *et al.* (LIGO Scientific Collaboration), Phys. Rev. D **72**, 062001 (2005).

[18] B. Abbott *et al.* (LIGO Scientific Collaboration), Classical Quantum Gravity **23**, S29 (2006).

[19] H. Takahashi *et al.* (TAMA Collaboration and LISM Collaboration), Phys. Rev. D **70**, 042003 (2004).

[20] B. Abbott *et al.* (LIGO Collaboration), Phys. Rev. D **73**, 102002 (2006).

[21] K. Cannon, arXiv:g070881-00-Z.

[22] C. Cutler and E. Flanagan, Phys. Rev. D **49**, 2658 (1994).

[23] L. Finn, Phys. Rev. D **46**, 5236 (1992).

[24] L. Finn and D. Chernoff, Phys. Rev. D **47**, 2198 (1993).

[25] D. F. Chernoff and L. S. Finn, Astrophys. J. **411**, L5 (1993).

[26] K. Kokkotas, A. Królak, and G. Tsegas, Classical Quantum Gravity **11**, 1901 (1994).

[27] A. Królak, K. Kokkotas, and G. Schäfer, Phys. Rev. D **52**, 2089 (1995).

[28] E. Poisson and C. Will, Phys. Rev. D **52**, 848 (1995).

[29] R. Balasubramanian, B. S. Sathyaprakash, and S. V. Dhurandhar, Pramana **45**, L463 (1995).

[30] R. Balasubramanian, B. S. Sathyaprakash, and S. V. Dhurandhar, Phys. Rev. D **53**, 3033 (1996); **54**, 1860(E) (1996).

[31] E. E. Flanagan and S. A. Hughes, Phys. Rev. D **57**, 4566 (1998).

[32] K. G. Arun, B. R. Iyer, B. S. Sathyaprakash, and P. A. Sundararajan, Phys. Rev. D **71**, 084008 (2005); **72**, 069903(E) (2005).

[33] S.-i. Amari and H. Nagaoka, *Methods of Information Geometry* (American Mathematical Society, Providence, RI, 2000).

[34] B. S. Sathyaprakash, Phys. Rev. D **50**, R7111 (1994).

[35] B. Owen, Phys. Rev. D **53**, 6749 (1996).

[36] B. Owen and B. S. Sathyaprakash, Phys. Rev. D **60**, 022002 (1999).

[37] C. Helström, *Statistical Theory of Signal Detection*, International Series of Monographs in Electronics and Instrumentation Vol. 9 (Pergamon Press, Oxford, U.K., 1968), 2nd ed.

[38] K. S. Thorne, in *Three Hundred Years of Gravitation*, edited by S. Hawking and W. Israel (Cambridge University Press, Cambridge, England, 1987), pp. 330–458.

[39] B. Schutz, in *The Detection of Gravitational Waves*, edited by D. Blair (Cambridge University Press, Cambridge, England, 1989).

[40] Y. Pan, A. Buonanno, Y. Chen, and M. Vallisneri, Phys. Rev. D **69**, 104017 (2004).

[41] L. S. C. Compact Binary Coalescence Group (private communication).

[42] J. Perram and M. Wertheim, J. Comput. Phys. **58**, 409 (1985).

[43] Wikipedia Article, Brent's Method, http://en.wikipedia.org/wiki/Brent's_method.

[44] R. Brent, *Algorithms for Minimization Without Derivatives* (Prentice-Hall, Englewood Cliffs, NJ, 1973), Chap. 4.

[45] GSL, http://www.gnu.org/software/gsl/ (The GNU Scientific Library is a free numerical library licensed under the GNU GPL).

[46] L. Blanchet, T. Damour, and B. R. Iyer, Phys. Rev. D **51**, 5360 (1995).

[47] L. Blanchet, T. Damour, B. R. Iyer, C. M. Will, and A. G. Wiseman, Phys. Rev. Lett. **74**, 3515 (1995).

[48] S. Babak, R. Balasubramanian, D. Churches, T. Cokelaer, and B. Sathyaprakash, Classical Quantum Gravity **23**, 5477 (2006).

[49] T. Cokelaer, Phys. Rev. D **76**, 102004 (2007).

[50] LSC Algorithm Library, http://www.lsc-group.phys.uwm.edu/daswg/projects/lal.html.